Macromolecules

pubs.acs.org/Macromolecules Article

Alternating Ring-Opening Metathesis Polymerization Provides Easy Access to Functional and Fully Degradable Polymers

Francis O. Boadi, Jingling Zhang, Xiaoxi Yu, Surita R. Bhatia, and Nicole S. Sampson*

Cite This: https://dx.doi.org/10.1021/acs.macromol.0c01051 Read Online

ACCESS | Metrics & More | Article Recommendations | Supporting Information

ABSTRACT: Polymers with hydrolyzable groups in their backbones have numerous potential applications in biomedicine, lithography, energy storage, and electronics. In this study, acetal and ester functionalities were incorporated into the backbones of copolymers by means of alternating ring-opening metathesis polymerization catalyzed by the third-generation Grubbs ruthenium catalyst. Specifically, combining large-ring (7−10 atoms) cyclic acetal or lactone monomers with bicyclo[4.2.0]oct-1(8)-ene-8-carboxamide monomers provided perfectly alternating copolymers with acetal or ester functionality in the backbones and low to moderate molecular weight distribution ($Đ_M$ = 1.2−1.6). Copolymers containing ester and acetal backbones hydrolyzed to significant extent under basic conditions (pH 13) and acidic conditions (pH ≤ 5), respectively, to yield the expected byproducts within 30 h at moderate temperature. Unlike the copolymer with an all-carbon backbone, copolymers with a heteroatom-containing backbone exhibited the viscoelastic behavior with crossover frequency, which decreases as the size of the R group on the acetal increases. In contrast, the glass transition temperature (T_g) decreases as the size of the R group decreases. The rate of hydrolysis of the acetal copolymers was also dependent on the R group. Thus, ruthenium-catalyzed alternating ring-opening metathesis copolymerization provides heterofunctional copolymers whose degradation rates, glass transition temperatures, and viscoelastic moduli can be controlled.

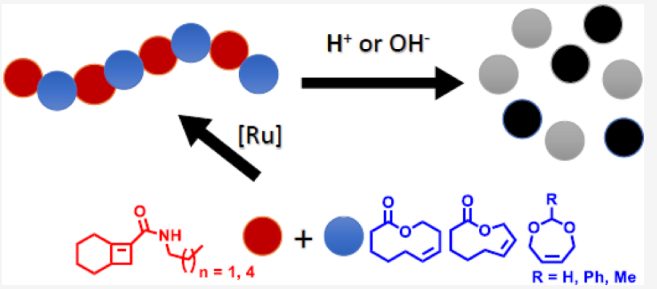

INTRODUCTION

Degradable polymers with hydrolyzable groups, such as esters and acetals, in their backbones have numerous applications in biomedicine,[1−4] lithography,[5,6] energy storage, and electronics.[7−9] However, simultaneously controlling the installation of appropriate functional units on the backbone and the sequential placement of the hydrolyzable groups by means of conventional polymerization methods is challenging. Polycondensation and transacetalation methods are widely utilized to synthesize polyacetal polymers,[3,10] and polycondensation and ring-opening polymerization are commonly used to synthesize ester-based polymers.[11] However, many polycondensation methods often yield low-molecular-weight polymers that lack important mechanical properties needed for certain applications; the metal alkoxide catalysts that are commonly employed for ring-opening polymerization have limited functional group tolerance.[12] Other conventional polymerization methods such as Suzuki polycondensation[5] and cationic copolymerization of vinyl ethers and conjugated aldehydes[13,14] show promise for providing access to degradable acetal polymers. In addition, ionic polymerization, atom transfer radical polymerization, reversible addition fragmentation chain transfer polymerization, and ring-opening metathesis polymerization (ROMP) are also robust techniques that provide control over polymer molecular weight and dispersity.

In the last three decades, ROMP has been championed for a wide range of applications in the life and materials sciences because the ruthenium catalysts used for ROMP exhibit excellent tolerance to many functional groups,[15,16] and, most important, the method provides good control over the molecular weight.[17−19] These features of ROMP have led to the development of diverse and useful material architectures.[20,21] However, owing to the heavy reliance on norbornene and norbornene derivatives as ROMP monomers, progress on the use of this method to prepare degradable[22−30] and sequence-defined polymers has been limited.[23,25] The research groups of Grubbs,[31] Kilbinger,[32,33] and O'Reilly[34] have reported that commercially available acetal-based cyclic olefins (dioxepins) can be used in ROMP systems to potentiate polymer degradation. However, their efforts were met with limited success because these cyclic olefins do not undergo controlled homopolymerization[31,35] or perfectly cross or alternating copolymerization with monomers such as

Received: May 3, 2020
Revised: June 25, 2020

https://dx.doi.org/10.1021/acs.macromol.0c01051
Macromolecules XXXX, XXX, XXX−XXX

Chart 1. Monomers and Catalyst Used for Alternating Copolymer and Diblock Copolymer Synthesis[a]

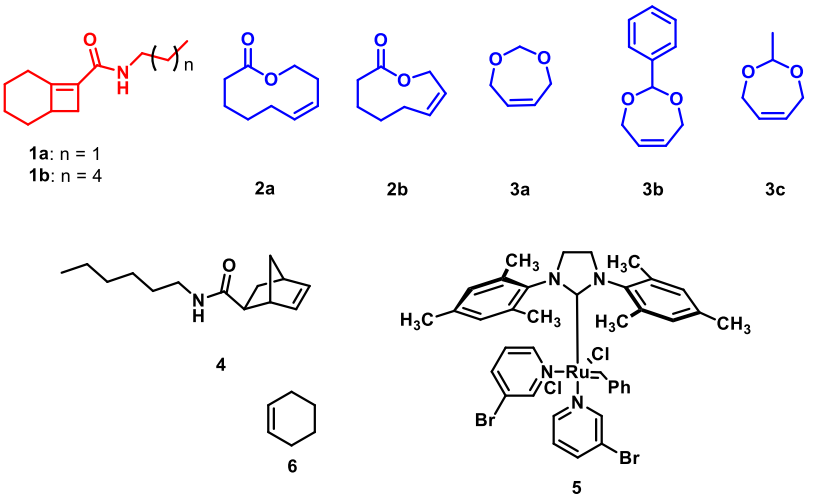

[a]Monomers **1**, **2**, and **3** were used for alternating copolymer synthesis, and monomer **4** was used for block copolymer synthesis. Third-generation Grubbs catalyst **5** was used for all the metathesis polymerization reactions. Monomer **6** was used to prepare **1a**-*alt*-**6**, an all carbon-backbone copolymer, for comparison.

cyclooctadiene and norbornene.[31,34] Even when used in excess, the dioxepins are scarcely incorporated. Utilization of functional dioxepins in ROMP does not give access to fully degradable polymers, although when a single monomer is added to a ROMP polymer chain, the dioxepin can be sacrificed to yield a chain-end functional group that serves as a handle for postpolymerization chain extension.[35−37]

Recent work on alternating ring-opening metathesis polymerization (AROMP) in which high-ring-strain and low-ring-strain olefin monomers undergo perfect alternating polymerization to yield long controlled polymers[38,39] inspired us to consider the use of heterocycles for the synthesis of degradable polymers. Our discovery that bicyclo[4.2.0]oct-1(8)-ene-8-carboxamides undergo AROMP with large cycloalkenes (10−12 carbon atoms)[40] suggested that large heterocyclic rings containing hydrolyzable linkages would also work in the new system (Chart 1). Contemporaneously, Xia and co-workers[41] demonstrated the efficient incorporation of dioxepins into copolymer backbones using their novel cyclopropene monomers in AROMP. Herein, we report the efficient synthesis of alternating, readily degradable ester and acetal copolymers by means of cyclobutene-based AROMP (Figure 1) with thermal properties and interfacial elasticity that are significantly different from the all-carbon backbone AROMP copolymers.[42]

RESULTS

Monomer Preparation. Monomer **1a** was synthesized by coupling bicyclo[4.2.0]oct-1(8)-ene-8-carboxylic acid with *N*-propylamine according to the literature procedure.[43] Column chromatography and recrystallization afforded **1a** in good isolated yield (>70%) and excellent purity (>95%, as indicated by ^{1}H NMR spectroscopy). Monomer **1b** was prepared analogously as previously described[43] with *N*-hexylamine in good yield (>65%) with excellent purity (>95%, as indicated by ^{1}H NMR spectroscopy). Monomer **2a** was obtained by means of the procedure described by Conrad et al.[44] Monomer **2a** was a mixture of cis and trans isomers and contained 10% olefin regioisomer that was inseparable from **2a**. Monomer **2b** was synthesized by the ring-closing metathesis of prop-2-enyl

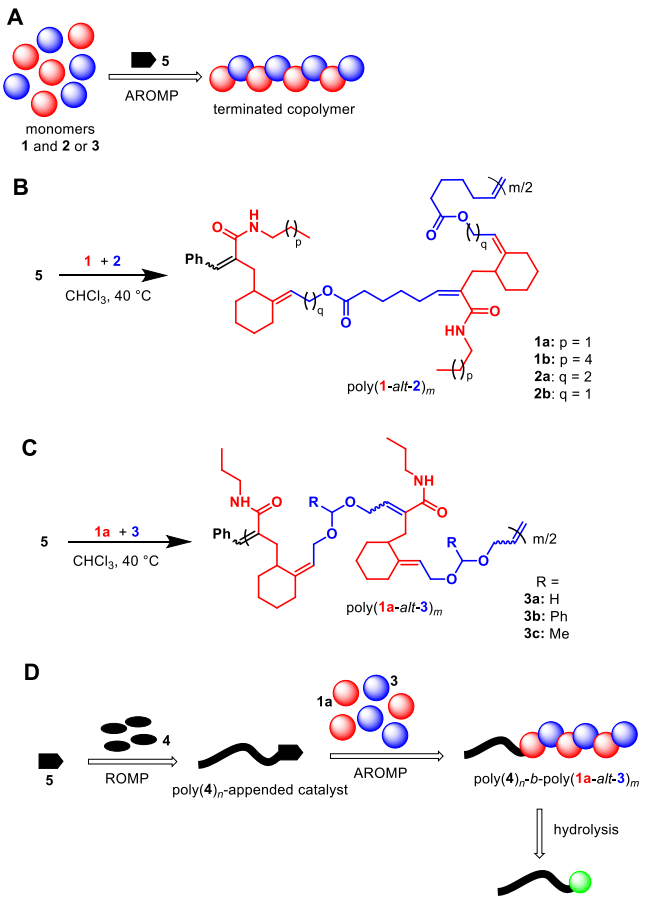

Figure 1. Synthesis of alternating and diblock copolymers. (A) Cartoon representation of alternating copolymer synthesis, (B) poly(**1**-*alt*-**2**)$_m$ synthesis where **1a** or **1b** was used together with **2a** or **2b** to form copolymers with **5** (10 mM), (C) poly(**1a**-*alt*-**3**)$_m$ synthesis with **5** (10 mM), and (D) cartoon representation of poly(**4**)$_n$-*b*-poly(**1a**-*alt*-**3**)$_m$ synthesis with **5** (25 mM) and subsequent hydrolytic degradation to afford poly(**4**)$_n$ with a functional end-group (green ball). *n* and *m* represent the repeat units.

https://dx.doi.org/10.1021/acs.macromol.0c01051
Macromolecules XXXX, XXX, XXX−XXX

Table 1. Average Molecular Weights and Molecular Weight Distributions ($Đ_M$) of Ester and Acetal Alternating Copolymers Prepared by AROMP[a]

entry	copolymer	[1]/[2,3]/[5] ratio	conv[b] (%)	time (h)	%[c]2/3	$M_{w,theo}$[d] (kDa)	M_n[e,g] (kDa)	M_w[f,g] (kDa)	$Đ_M$	M_n[i] (kDa)
1	(**1a**-*alt*-**2a**)$_{10}$	10:10:1	100	5	48	3.50	4.80	7.40	1.5	4.2
2	(**1a**-*alt*-**2a**)$_{50}$	50:50:1	100	18	49	17.3	20.8	27.7	1.3	24.0
3	(**1a**-*alt*-**2b**)$_{10}$	10:10:1	100	5	48	3.30	5.10	7.60	1.5	7.4
4	(**1a**-*alt*-**2b**)$_{50}$	50:50:1	100	18	46	16.6	12.7	20.2	1.6	22.6
5	(**1b**-*alt*-**2a**)$_{10}$	10:10:1	100	8	51	3.90	4.30	6.60	1.5	5.9
6	(**1b**-*alt*-**2b**)$_{10}$	10:10:1	100	8	49	3.80	6.00	9.80	1.6	5.7
7	(**1b**-*alt*-**2b**)$_{50}$	50:50:1	100	21	42	18.8	16.2	24.7	1.5	19.9
8	(**1a**-*alt*-**3a**)$_{20}$	20:20:1	100	1.5	52	5.89	6.92	10.1	1.5	6.16
9	(**1a**-*alt*-**3a**)$_{50}$	50:50:1	100	2.5	53	14.6	12.5	15.6	1.2	17.0
10	(**1a**-*alt*-**3a**)$_{100}$	100:100:1	85	5	51	24.9[h]	15.5	24.2	1.6	29.1
11	(**1a**-*alt*-**3b**)$_{20}$	20:40:1	100	2.5	47	8.78	7.49	9.32	1.2	7.39
12	(**1a**-*alt*-**3b**)$_{50}$	50:100:1	65	19	50	12.0[h]	11.9	17.2	1.4	12.2
13	(**1a**-*alt*-**3b**)$_{100}$	100:200:1	55	19	48	20.3[h]	13.2	20.3	1.5	18.5
14	(**1a**-*alt*-**3c**)$_{20}$	20:20:1	100	2	50	6.14	4.38	5.88	1.3	6.76
15	(**1a**-*alt*-**3c**)$_{50}$	50:90:1	100	2.5	52	15.4	5.37	8.06	1.5	18.4

[a]AROMP was performed with catalyst **5** (10 mM) at 40 °C in CH_2Cl_2 or $CHCl_3$. [b]Conversion was determined by the integration of the cyclohexyl peak at 2.8 ppm in the ^{1}H NMR spectrum. [c]Percent composition of lactone **2** or dioxepin **3** in copolymers. [d]Theoretical molecular weight was calculated from the monomer/catalyst feed ratio. [e]Number average molecular weight (M_n) was determined by GPC with polystyrene standard calibration. [f]Weight average molecular weight (M_w) was determined by GPC with polystyrene standard calibration. [g]Polymers were analyzed by GPC on a Phenogel 5 μm 10E4A LC column (300 × 7.8 mm, 5−500 kDa MW) with THF as the eluent at a flow rate of 0.7 mL/min at 30 °C. [h]Theoretical molecular weight after adjustment for conversion. [i]Determined by phenyl end-group analysis by means of ^{1}H NMR spectroscopy.

hept-6-enoate; the complete consumption of the starting material was confirmed by the disappearance of the alkene proton signals at 5.3−4.9 ppm in the ^{1}H NMR spectrum (Figures S1 and S2). The product was a 70:30 mixture of cis and trans isomers. Dioxepin monomer **3a** was purchased from Sigma-Aldrich and used as received. Monomers **3b** and **3c** were synthesized from *cis*-2-butene-1,4-diol and benzaldehyde or acetaldehyde, respectively, as described in the literature[34] and were microdistilled to give the desired products in >98% purity (as indicated by ^{1}H NMR spectroscopy, Figures S3 and S4) and in good yield (80%). Monomer **4** was synthesized in 93% isolated yield by coupling *exo*-5-norbornenecarboxylic acid with *N*-hexylamine.[43]

Test for Monomer Homopolymerization. Monomers **1** do not undergo homopolymerization (ROMP) in the presence of third-generation Grubbs catalyst **5** (Chart 1).[38] We hypothesized that they would undergo AROMP with a cyclic olefin that has low ring strain and does not undergo **5**-catalyzed ROMP, or does so extremely slowly. To evaluate this hypothesis, we subjected solutions of **2** (125 mM) and **3** (250 mM) to catalyst **5** (12.5 mM) at temperatures of 30−40 °C. As observed by ^{1}H NMR spectroscopy, **2** did not homopolymerize over 24 h (Figure S5), nor did monomer **3**. However, **3a** and **3c** underwent olefin isomerization; specifically, double bond migration generated thermodynamically more stable cyclic vinyl ether products **3a′** and **3c′** (Figures S6 and S7). Isomerization of monomer **3b** was much slower or barely occurred (Figure S8).

Preparation of Ester and Acetal Alternating Copolymers by AROMP of Monomers 1 with Monomers 2 or 3. When monomer **1a** or **1b** was allowed to react with **2a** or **2b** at 40 °C in the presence of catalyst **5** (10 mM), all combinations resulted in the formation of linear alternating copolymers poly(**1**-*alt*-**2**)$_m$ with ester linkages in the polymer backbone (Table 1, entries 1−7). The reactions of both **1a** and **1b** were robust enough to form long chains (50 repeating **1**-*alt*-**2**), and molecular weight distributions were acceptable. Monomer **2a** contained an olefin regioisomer that also polymerizes with monomer **1**. Thus, a complex polymeric backbone structure was formed. Three copolymers with **2a** were synthesized (Table 1, entries 1, 2 and 5) demonstrating that the regioisomer does not impede AROMP and **2a** forms alternating copolymers at least 50 repeating **1**-*alt*-**2a** units long. Monomer **1a** was slightly more reactive than **1b**; we infer that the shorter side chain decreased steric hindrance in the metathesis reaction.

Two regioisomeric structures are proposed for alternating copolymer poly(**1b**-*alt*-**2b**)$_{10}$ and poly(**1b**-*alt*-**2b**)$'_{10}$ on the basis of analysis by ^{1}H−^{1}H COSY (Figure 2), ^{1}H, ^{13}C and HSQC NMR spectroscopy (Figures S9−S11). COSY indicated that H4 and H5 were neighbors and that H1′ was coupled to H5′. No correlation was seen between H4′ and H5′ or between H1 and H5. Taken together, these results indicate that poly(**1b**-*alt*-**2b**)$_m$ accounted for approximately two-thirds of the polymer backbone structure and poly(**1b**-*alt*-**2b**)$'_m$ accounted for approximately one-third. Poly(**1a**-*alt*-**2b**)$_m$ exhibited regioisomerism in its backbone because **2b** could ring open and coordinate with Ru alkylidene in two different ways.

Alternating copolymers poly(**1a**-*alt*-**3a**)$_m$ were synthesized from equimolar mixtures of **1a** and **3a** with catalysis by **5** (10 mM, Table 1, entries 8−10). However, poly(**1a**-*alt*-**3b**)$_m$ copolymers with near theoretical molecular weights were obtained using a twofold excess of monomer **3b** with respect to **1a** (Table 1, entries 11−13). We noted a slight decomposition of **3b** during the reaction, evident by the appearance of aldehyde peak at 10 ppm in the ^{1}H NMR spectrum of the reaction mixture; the use of excess **3b** compensated for the molar loss due to decomposition. The reaction between monomers **3b** and **1a** was relatively slow; the preparation of higher-molecular-weight polymers required longer reaction time (19 h), and monomer conversion was only slightly higher than 50% (Table 1, entries 12 & 13). Poly(**1a**-*alt*-**3c**)$_m$ copolymers were synthesized following a protocol similar to

https://dx.doi.org/10.1021/acs.macromol.0c01051
Macromolecules XXXX, XXX, XXX−XXX

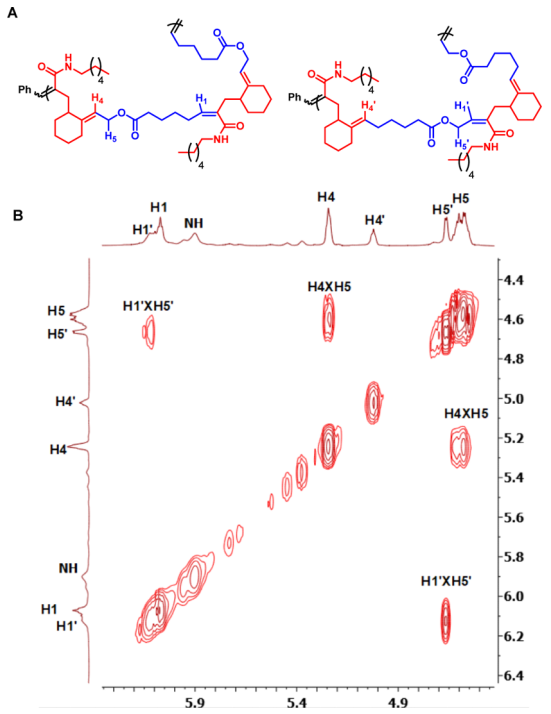

Figure 2. (A) Proposed structures of poly(**1b**-*alt*-**2b**)$_{10}$ (left) and poly(**1b**-*alt*-**2b**)$'_{10}$ (right), (B) partial ^{1}H−^{1}H COSY NMR spectrum of a mixture of the two regioisomers.

that used for poly(**1a**-*alt*-**3a**)$_m$ (Table 1, entries 14−15). The molecular weights and distributions of the copolymers were determined by gel permeation chromatography (GPC) and ^{1}H NMR endgroup analysis. For higher degrees of polymerization (DP), especially DP ≥ 50, only MWs measured by ^{1}H NMR were similar to the theoretical molecular weights. DP refers to the total number of alternating AB pairs in the polymer. All the synthesized copolymers had moderate molecular weight distributions ($Đ_M$), with $Đ_M$ values ranging from 1.2 to 1.6 and near stoichiometric incorporation of the comonomers suggesting efficient alternation (Table 1). In the matrix-assisted laser desorption ionization time-of-flight (MALDI-TOF) mass spectrum of the **1a**-*alt*-**3a** copolymer (Figure S12) there is an absence of mass shifts corresponding to **3a**−**3a** diads, consistent with the clear alternation of **1a** and **3a** in the copolymer.

We examined the kinetics of AROMP versus isomerization by ^{1}H NMR spectroscopy. The half-lives of **3a** and **1a** for AROMP were 20 and 23 min, respectively, which indicates that both **1a** and **3a** are incorporated into the copolymer at almost equal rates during copolymerization (Figure S13); whereas the half-life of **3a** isomerization was 203 min (Figure S14). To suppress **3a**′ formation, 1,4-benzoquinone was used as an additive (Figure S15). Moreover, AROMP reaction involving **1a** and **3a** in the presence of 1,4-benzoquinone yielded a copolymer, which had identical ^{1}H and HSQC NMR spectra as the copolymer prepared without the additive (Figures S16), which is consistent with poly(**1a**-*alt*-**3a**)$_m$ rather than poly(**1a**-*alt*-**3a**′)$_m$.

Hydrolytic Degradation of Ester and Acetal Alternating Copolymers. Surprisingly, the ester and acetal copolymers exhibited different solubility profiles; hence, different hydrolysis protocols were applied for these two categories of polymers. Ester-alternating copolymers were subjected to hydrolysis in aqueous solution at several pH values. Poly(**1**-*alt*-**2a**)$_m$ was not included in the degradation studies because of its complex backbone structure introduced by regioisomers in the monomer **2a**. Copolymers, poly(**1**-*alt*-**2b**)$_m$ were readily hydrolyzed under strongly basic conditions; at pH 13, 78% of poly(**1a**-*alt*-**2b**)$_{10}$ and 26% of poly(**1b**-*alt*-**2b**)$_{10}$ were degraded within 8 h (Figure S17). However, under mildly acidic conditions or mildly basic conditions, these **2b**-based copolymers exhibited slow to no degradation. The alkaline degradation products, which were soluble in the aqueous phase, were purified by high-performance liquid chromatography (HPLC); the eluates were analyzed by mass spectrometry and the expected hydroxy acid degradation product was observed (Figure S17). The mass spectrum did not reveal evidence of homoaddition of **1** to form dimer or trimer. Copolymers containing propyl amide side chain, **1a** had a much faster degradation rate than **1b**, which has the hexyl amide. This result is expected because the lower hydrophobicity of **1a** allows for better solvation of its copolymers. Therefore, **1a**-containing copolymers were used for all subsequent degradation testing.

For acetal alternating copolymers, poly(**1a**-*alt*-**3**)$_m$, we began by exploring hydrolysis under mildly acidic conditions (sodium phosphate buffer, pH 5). Under these conditions, the poly(**1a**-*alt*-**3a**)$_{20}$ copolymer was inert to hydrolytic degradation, even after several days (Figure S18). However, poly(**1a**-*alt*-**3b**)$_{20}$ underwent significant hydrolysis and the time scale was hours (Figures 3; S19). When the degraded crude mixture of

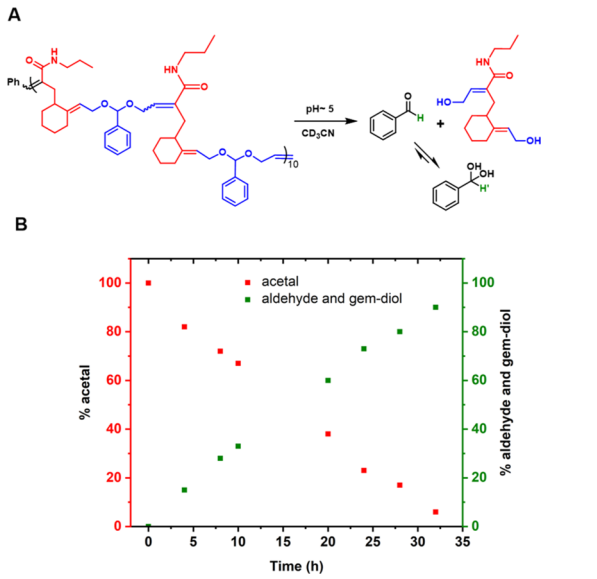

Figure 3. Poly(**1a**-*alt*-**3b**)$_{20}$ underwent complete degradation within 30 h at pH 5. (A) Acetal copolymer degradation reaction scheme, (B) acetal hydrolysis and benzaldehyde formation at 37 °C, pH 5.

poly(**1a**-*alt*-**3b**)$_{20}$ was analyzed by mass spectroscopy, peaks: m/z = 107.0 $[M + H]^+$, corresponding to benzaldehyde (exact mass = 106.4 g/mol), and m/z = 305.1−308.2 $[M + Na + H]^+$, which we attributed to diallyl alcohol (exact masses = 281.20 and 283.21 g/mol for OH and OD, respectively) were observed (Figure S20). Similar to **1**−**2**-based copolymers, there was no evidence of homoaddition of **1a** in the **5**-catalyzed reaction of **1a** and **3** monomers, which confirms that efficient alternation occurs.

https://dx.doi.org/10.1021/acs.macromol.0c01051
Macromolecules XXXX, XXX, XXX−XXX

Preparation and Hydrolytic Degradation of Diblock Copolymers. A nondegradable norbornene polymer block, poly(**4**)$_n$, was extended with a degradable poly(**1a**-*alt*-**3**)$_m$ block to afford poly(**4**)$_n$-*b*-poly(**1a**-*alt*-**3**)$_m$ (Scheme 1). Upon extension of the chain with the second block, the molecular weight of the polymer increased (Figures 4 and 5). According to the number average molecular weight determined by GPC (Table 2, entry 2) approximately 12 units of (**1a**-*alt*-**3a**) were installed onto poly(**4**)$_{20}$ to yield the diblock copolymer, poly(**4**)$_{20}$-*b*-poly(**1a**-*alt*-**3a**)$_{12}$ (Figure 4A). (**1a**-*alt*-**3a**) copolymer is hydrolytically inert at pH 5, so we employed relatively stronger acidic conditions to induce degradation; the diblock copolymer was treated with aqueous trifluoroacetic acid (TFA, pH 1) at 37 °C for ∼7 days. This treatment resulted in a loss of ∼67% of the installed poly(**1a**-*alt*-**3a**)$_{12}$ block (Figure 4A; Table 2, entry 3). Partial degradation of the (**1a**-*alt*-**3a**)$_{12}$ block of the diblock copolymer was hardly detected by ^{1}H NMR spectroscopy (Figure S21).

We next explored the hydrolysis rate of the (**1a**-*alt*-**3b**) copolymer in a diblock copolymer system. A block of (**1a**-*alt*-**3b**)$_{10}$ was successfully installed onto poly(**4**)$_{20}$ to form a diblock copolymer poly(**4**)$_{20}$-*b*-(**1a**-*alt*-**3b**)$_{10}$ (Figure 5; Table 2, entry 8). This diblock copolymer was treated under two different acidic conditions (thus pH 1 & 5) at 37 °C. Incubation of this diblock copolymer in sodium phosphate buffer (pH 5) for 68 h resulted in a nearly 60% loss of the poly(**1a**-*alt*-**3b**)$_{10}$ block (Table 2, entry 9). At pH 1 (TFA condition), the poly(**1a**-*alt*-**3b**)$_{10}$ block is completely hydrolyzed within 46 h to yield a new poly(**4**)$_{20}$, as indicated by GPC (Figure 5; Table 2, entry 10) and ^{1}H NMR spectroscopy (Figure S21).

Inspired by the degradation rates observed for the diblock copolymers containing poly(1a-*alt*-**3a**/**b**)$_m$, we explored substituent effects on the degradation rate. We anticipated that acetaldehyde-derived copolymer poly(**1a**-*alt*-**3c**)$_m$ would hydrolyze faster than the formaldehyde-derived poly(**1a**-*alt*-**3a**)$_m$. Therefore, we prepared diblock copolymer poly(**4**)$_{20}$-*b*-poly(**1a**-*alt*-**3c**)$_{10}$ (Figure 4B; Table 2, entry 4). Notably, the installation of poly(**1a**-*alt*-**3c**) (R = Me) onto poly(**4**)$_{20}$ was much faster than the installation of poly(**1a**-*alt*-**3b**) (R = Ph), but not as fast as that of poly(**1a**-*alt*-**3a**) (R = H); this trend is consistent with the relative sizes of the R groups. Poly(**4**)$_{20}$-*b*-poly(**1a**-*alt*-**3c**)$_{10}$ was subjected to hydrolytic degradation under two different sets of acidic conditions (pHs 1 & 5). Interestingly, when this diblock copolymer was treated with sodium phosphate buffer (pH 5), only 50% of the poly(**1a**-*alt*-**3c**)$_m$ block was hydrolyzed within 68 h (Figure 4B; Table 2,

Scheme 1. Synthesis of Poly(4)$_n$-*b*-poly(1a-*alt*-3)$_m$ and Hydrolytic Degradation of the Poly(1a-*alt*-3)$_m$ Blocks at pH ≤ 5

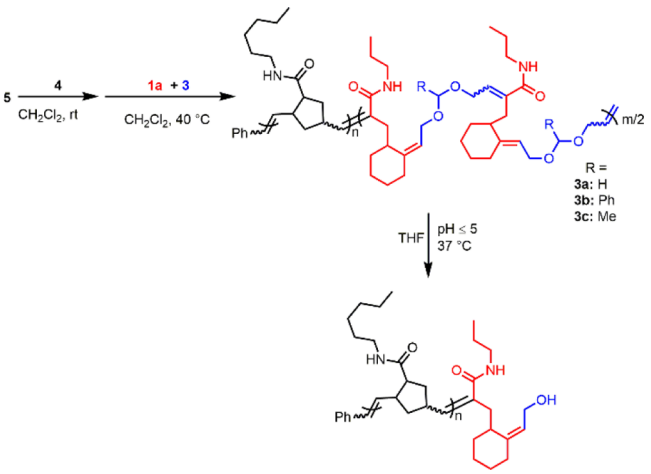

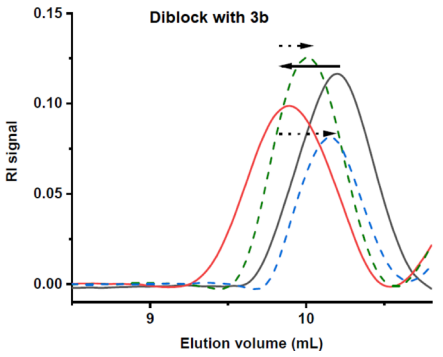

Figure 5. GPC analysis of block copolymer poly(**4**)$_{20}$-*b*-(**1a**-*alt*-**3b**)$_{10}$ before and after hydrolytic degradation under different acidic conditions. Installation of poly(**1a**-*alt*-**3b**)$_{10}$ onto poly(**4**)$_{20}$ (black line) yields diblock copolymer poly(**4**)$_{20}$-*b*-(**1a**-*alt*-**3b**)$_{10}$ (red line). Partial degradation (60%) of the (**1a**-*alt*-**3b**)$_{10}$ block at pH 5 for 68 h (dashed green line), and the complete degradation of (**1a**-*alt*-**3b**)$_{10}$ block at pH 1 for 46 h (dashed blue line). Horizontal arrows represent an increase (solid) or a decrease (dotted) in the MW.

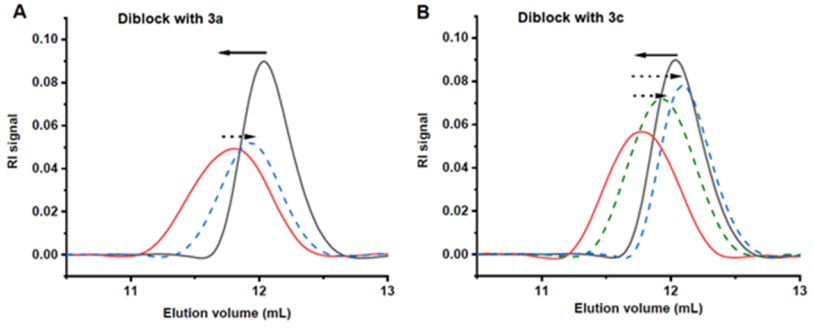

Figure 4. GPC analysis of MW shifts associated with the assembly and hydrolysis of block copolymers, 10−12 units of (**1a**-*alt*-**3**) were successfully installed onto poly(**4**)$_{20}$ (black line) to form a diblock copolymer (A) poly(**4**)$_{20}$-*b*-poly(**1a**-*alt*-**3a**)$_{12}$ (red line) or (B) poly(**4**)$_{20}$-*b*-poly(**1a**-*alt*-**3c**)$_{10}$ (red line). After treatment of the diblock copolymers with aqueous TFA (pH 1) at 37 °C (dashed blue line) (A) for 161 h, (**1a**-*alt*-**3a**) unit is partially hydrolyzed to yield poly(**4**)$_{20}$ with a new end group, (B) 46 h, (**1a**-*alt*-**3c**) unit degrades completely. At pH 5 only (**1a**-*alt*-**3c**) degrades (dashed green line). Horizontal arrows represent an increase (solid) or decrease (dotted) in the MW.

https://dx.doi.org/10.1021/acs.macromol.0c01051
Macromolecules XXXX, XXX, XXX−XXX

Table 2. Molecular Weights of Poly(**4**)$_{20}$ and Diblock Copolymers Consisting of Poly(**4**)$_{20}$ and Poly(**1a**-*alt*-**3**)$_m$ before and after Hydrolysis[a,b]

entry	pH & time of treatment	polymer	M_n (kDa)	M_w (kDa)	$Đ_M$
1	N/A[c]	poly(**4**)$_{20}$ block	4.48	5.50	1.23
2	N/A	poly(**4**)$_{20}$-*b*-(**1a**-*alt*-**3a**)$_{12}$ before hydrolysis	8.04	11.51	1.43
3	1.0 (161 h)	poly(**4**)$_{20}$-*b*-(**1a**-*alt*-**3a**)$_{12}$ after hydrolysis	5.64	7.47	1.33
4	N/A	poly(**4**)$_{20}$-*b*-(**1a**-*alt*-**3c**)$_{10}$ before hydrolysis	7.58	11.3	1.49
5	5.0 (68 h)	poly(**4**)$_{20}$-*b*-(**1a**-*alt*-**3c**)$_{10}$ after hydrolysis	5.92	8.17	1.38
6	1.0 (46 h)	poly(**4**)$_{20}$-*b*-(**1a**-*alt*-**3c**)$_{10}$ after hydrolysis	4.27	5.21	1.22
7	N/A	poly(**4**)$_{20}$	3.89	5.45	1.40
8	N/A	poly(**4**)$_{20}$-*b*-(**1a**-*alt*-**3b**)$_{10}$ before hydrolysis	7.86	11.6	1.48
9	5.0 (68 h)	poly(**4**)$_{20}$-*b*-(**1a**-*alt*-**3b**)$_{10}$ after hydrolysis	5.89	8.10	1.38
10	1.0 (46 h)	poly(**4**)$_{20}$-*b*-(**1a**-*alt*-**3b**)$_{10}$ after hydrolysis	4.15	5.72	1.38

[a]Values were determined using polystyrene standards and combined columns: a Phenogel 5 μm linear (2) LC column (300 × 7.8 mm, 100−10,000 kDa MW) and a Phenogel 5 μm, 50 Å LC column (300 × 4.6 nm, 100 Da to 3 kDa MW) with THF as the eluent at a flow rate of 0.7 mL/min at 30 °C (entries 1−6; Figure 4). [b]Values were determined using polystyrene standards and Phenogel 5 μm linear (2) LC column (300 × 7.8 mm, 100−10,000 kDa MW) with THF as the eluent at a flow rate of 0.7 mL/min at 30 °C (entries 7−10; Figure 5). [c]N/A: not applicable.

entry 5); whereas the treatment with aqueous TFA (pH 1) resulted in complete degradation within 46 h (Table 2, entry 6; Figures 4B & S21).

The GPC data clearly indicate that the AROMP acetal copolymer prepared from **3c** hydrolyzed much faster than **3a**, but slightly slower than that of **3b**. Unlike poly(**1a**-*alt*-**3a**)$_m$, poly(**1a**-*alt*-**3b**)$_m$ and poly(**1a**-*alt*-**3c**)$_m$ hydrolyzed to a considerable extent under mildly acidic conditions, and completely at pH 1. The hydrolysis rates paralleled the stabilities of the carboxonium-like ion intermediates[3] formed during hydrolysis with formaldehyde (**3a**) < acetaldehyde (**3c**) < benzaldehyde (**3b**).

Thermal Properties and Interfacial Elasticity of AROMP Polymers. We assessed copolymers comprising approximately 50 repeating comonomer units. We used differential scanning calorimetry (Figure S22), thermogravimetric analysis (Figure S23), and interfacial rheology (Figures 6, S24, and S25) to evaluate the processing properties and potential applications including the stability of the multiphase formulation of these copolymers. To elucidate the effects of the backbone heteroatoms, we compared the current generation of copolymers (those shown in Figure 1C) with one of our first-generation copolymers, poly(**1a**-*alt*-**6**),[42] where **6** is cyclohexene. Interfacial rheology was utilized because previous studies of related polymers[42] indicated an interesting behavior in the water-polymer film contact angle. This suggests a possible formation of self-assembled structures at the air−water interface during the drying of films. Data from strain amplitude sweeps (Figure S24) and time-dependent measurements (Figure S25) demonstrate that the samples are in the linear viscoelastic regime and the interfaces have come to

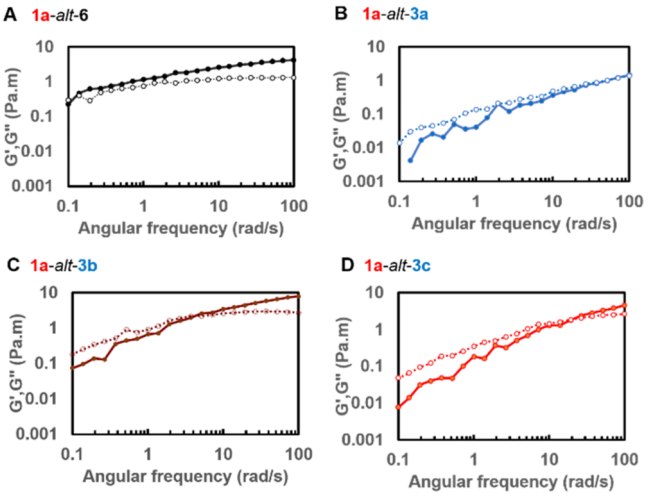

Figure 6. Interfacial rheology comparing the viscous and elastic properties of interfacial films of poly(**1a**-*alt*-**3**)$_{50}$ and poly(**1a**-*alt*-**6**)$_{50}$. The cyclohexene-based copolymer (A) displays a gel-like behavior with $G' > G''$ over the measurable frequency range, whereas the dioxepin-based copolymers (B−D) are viscoelastic with a crossover of G' and G' at intermediate frequencies of 3−60 rad/s, indicating timescales for the stress relaxation of the interface of 0.1−2 s, depending upon the R group. Solid lines, storage modulus (G'): dotted lines, loss modulus (G'').

equilibrium before oscillatory shear experiments were performed. Interfacial rheology, rather than bulk solution rheology, is the appropriate technique to explore this phenomenon. Additionally, as noted below, interfacial viscoelasticity is important to a number of applications, including the stability of multiphase formulations.[45] We found that acetal copolymers poly(**1a**-*alt*-**3**)$_{50}$ exhibited the viscoelastic behavior, with a crossover between the loss modulus G'' (indicative of viscous character) and the storage modulus G' (indicative of elastic character) as frequency was increased. Moreover, the crossover frequency for the **3a** copolymer was near the upper limit of the measurements at ∼60 rad/s, while the **3c** and **3b** copolymers displayed crossovers at ∼10 and ∼3 rad/s, respectively (Figure 6). The poly(**1a**-*alt*-**6**)$_{50}$, which has an all-carbon backbone, was dominated by the elastic behavior, with $G' > G''$ over the measurable frequency range. Ester-based copolymers (**1a**-*alt*-**2**) exhibited a flow behavior that is similar to the acetal copolymers and displayed a crossover at higher frequencies. Among the copolymers, poly(**1a**-*alt*-**6**)$_{50}$ had a higher G' and G'' than its acetal-based counterparts. Although the moduli are frequency-dependent, as would be expected for viscoelastic interfaces, over nearly all of the measurable frequency range, the storage modulus G' of the acetal copolymers increased as the size of the R group on the acetal carbon increased. That is, poly(**1a**-*alt*-**3b**)$_{50}$, which has a phenyl substituent, had the highest G', whereas poly(**1a**-*alt*-**3a**)$_{50}$ with hydrogen substituent has the lowest G' over the measurable frequency range. It was not possible to obtain the high-frequency plateau modulus because of instrument inertia effects. We also could not obtain data at lower frequencies to characterize the terminal regime, as data taken in this regime were below the limit of the torque transducer on the rheometer.

Copolymer with poly(**1a**-*alt*-**6**)$_{50}$ has the highest glass transition temperature T_g and decomposition temperature T_{dec}. Of the acetal copolymers, **3a**-containing copolymer had

https://dx.doi.org/10.1021/acs.macromol.0c01051
Macromolecules XXXX, XXX, XXX−XXX

the lowest T_g (7.7 °C), yet the most thermally stable (T_{dec} ~237 °C). Interestingly, there appeared to be a direct correlation between moduli and T_g. Thus, as the T_g increased, the modulus increased with **6** > **3b** > **3c** > **3a**.

DISCUSSION

Reactivity of Heteroatom-Containing Large Rings, 2 and 3, with Catalyst 5. Monomers **2** and **3** are excellent substrates for AROMP with monomer **1**. We recognized that some of these monomers undergo competing reactions or contained inseparable regioisomers. Therefore, we undertook investigation of their reactivity and characterization of the final copolymer structures to determine the best copolymer candidates for exploring degradation and material properties.

Because of the structural complexity associated with **2a** copolymers (Figures S26 and S27), arising from the presence of the inseparable 9-hydroxy-7-nonenoic acid lactone impurity, we devised monomer **2b** in the hope that the close proximity of the alkene to the ester functional group would increase steric hindrance and suppress olefin isomerization. However, **2b** contained cis/trans-isomeric mixtures, both of which undergo AROMP to yield regioisomerically complex copolymers (Figure 2). Hence, we did not pursue further extensive studies with monomers **2**.

We then moved to the exploration of the dioxepin monomers **3**. Because of their symmetrical structures, we anticipated they would yield structurally regular copolymers. However, **3a** and **3c** readily form **3a′** and **3c′** in the presence of **5**. This isomerization process is most likely catalyzed by a ruthenium hydride species generated by catalyst decomposition.[46] Because of the twist boat conformation of dioxepins,[47] intramolecular aryl-vinyl π-stacking interactions in **3b**[48] sterically hinder olefin isomerization. We were concerned that the copolymer microstructure would be irregular should the isomerization products participate in AROMP. Alternatively, **3′** are vinyl ethers and could act as terminating agents to quench the polymerization prematurely. Fortunately, the rate of isomerization of **3a** to **3a′** was approximately 1/10 the rate of consumption of **3a** in AROMP. This rate difference suggests that AROMP of **3a** competes effectively with isomerization to **3a'**. To confirm the reactivity ratios, we added 1,4-benzoquinone[49] to suppress ruthenium hydride (Figure S15). There was no structural difference as detected by NMR spectroscopy and we concluded that monomers **3** can be used effectively in AROMP.

In most cases, a degree of polymerization (DP_n) ≈100 was achieved. Molecular weights determined using GPC with polystyrene standards were significantly different than molecular weights determined by ^{1}H NMR endgroup analysis. The latter gave MW values that were comparable with the theoretical MW, and consistent with complete monomer consumption. Because our polymers are linear with backbones significantly different from the polystyrene standards, the MW may be underestimated by GPC,[50] except in the case of poly(**1a**-*alt*-**3b**)$_n$, which contains aromatic rings similar to the calibration standards. The complete monomer consumptions during the copolymerization of **2**, **3a**, and **3c**, further suggests MWs may be underestimated by GPC.

Hydrolytic Degradation of Ester and Acetal Copolymers. Hydrolytic degradation experiments were conducted over a wide pH range. Poly(**1a**-*alt*-**2**)$_m$ and poly(**1b**-*alt*-**2**)$_m$ underwent degradation under basic conditions, but degradation was relatively slow. Extreme pH-accelerated degradation, and at pH 13, these polymers were degraded completely within 24 h as expected.[51] In contrast, they were almost completely inert under mildly acidic conditions (pH 5). The acetal-based copolymers degraded substantially under acidic conditions (pH ≤ 5).[3,52] Because copolymers containing **3** had more regular backbones, we focused the remainder of our work on the dioxepin-derived copolymer series.

The kinetics of poly(**1a**-*alt*-**3b**)$_{20}$ hydrolysis revealed a constant rate of benzaldehyde release (Figure 3B). This feature makes this copolymer a candidate for applications, in which controlled-sustained release of a cargo is desired.[53] The clean-readable mass spectrum of the degraded mixture also suggests that hydrolytic degradation has potential utility as a tool for sequencing nontemplated sequence-controlled copolymers.[54] We prepared blocks of degradable and nondegradable polymers to more readily characterize the process of hydrolysis. At pH ≤ 5, free poly(**1a**-*alt*-**3b**)$_{20}$ degraded twice as fast as poly(**1a**-*alt*-**3b**)$_{10}$ in the diblock copolymer. The diblock copolymer may undergo phase separation because of the difference in the hydrophobicities of the poly(**4**)$_{20}$ block (hydrophobic) and the poly(**1a**-*alt*-**3b**)$_{10}$ block (more hydrophilic),[55] which could be expected to decrease the interaction of the poly(**1a**-*alt*-**3b**)$_{10}$ block with the aqueous acidic medium and hamper its hydrolysis.[3]

Diblock copolymer design revealed another important physical characteristic of the hetero-atom AROMP block (**1a**-*alt*-**3**). We noted that poly(**4**)$_{20}$ was not readily soluble in tetrahydrofuran (THF). However, when the chain was extended with poly(**1a**-*alt*-**3**)$_m$, the resulting polymer dissolved readily. This result suggests that the copolymers with heteroatom-containing backbones act not only as degradable blocks but also as solubilizing units.

Thermal Properties and Interfacial Elasticity of Carbon and Acetal Backbone Copolymers. Our interfacial rheology data show that all acetal copolymer films display the viscoelastic behavior with a crossover frequency that is dependent on the R group and increases as **3a** > **3c** > **3b**, indicating the fastest dynamics for R = H, followed by R = Me and R = Ph. Because timescales for the relaxation of mechanical stress are inversely proportional to the crossover frequency, this indicates that the timescale for mechanical relaxation increases with the size of the R group, which is physically reasonable. We note that, although these samples have varying molecular weights, the interfacial rheology experiments are all conducted on polymers with 50 backbone repeat units. So, any differences in the polymer molecular weight are due to differences in the molecular weight of the substituent groups, and impacts on the rheology can be attributed to size of the R groups. As the stability of multiphase formulations is directly impacted by interfacial rheology, the variation in G' and crossover frequency that we observe may serve as a useful means of tuning release in applications such as emulsion-based injectables. By contrast, the relaxation of the cyclohexene-based copolymer poly (**1**-*alt*-**6**)$_m$ was dominated by the elastic response over the accessible frequency range. We believe the elasticity in the acetal copolymers arises from interchain hydrogen boding[56,57] owing to the oxygen atoms. Copolymers with higher T_g, particularly those containing **6** and **3b**, also tend to have higher moduli, which is indicative of a less-flexible backbone.[58] Although the **3a** (R = H) acetal copolymer is least susceptible to hydrolytic degradation, it has significantly higher thermal stability. Moreover, as a polyoxymethylene-like material, **3a**-polymer can be used as a polymer

https://dx.doi.org/10.1021/acs.macromol.0c01051
Macromolecules XXXX, XXX, XXX−XXX

blend with polylactide to increase its flexural strength and modulus.[59]

CONCLUSIONS

A polymer's thermal properties, such as glass transition temperature (T_g) and decomposition temperature (T_{dec}), are crucial for material processing,[60] and its interfacial rheological properties are important for applications such as coatings and multiphase formulations. We have developed a new class of functional alternating copolymers that demonstrate the versatility of the AROMP method to efficiently incorporate oxygen functionality into the copolymer backbone. Substitution at the 2-position in poly(**1**-*alt*-**3b**)$_m$ and poly(**1**-*alt*-**3c**)$_m$ allows control of the stereochemistry of the double bonds in the polymer backbone, the rate of hydrolytic degradation, fine-tuning of physical properties such as T_g and T_{dec}, and interfacial rheology. Thus, the processing of films and coatings and stability of multiphase formulations can be adjusted. In addition, the precise incorporation of hydrolyzable monomeric units in the polymer backbone allows for controlled degradation that will be useful for reading sequence and analyzing precision in nontemplated copolymers. We anticipate polymers based on these copolymer structures will find applications in data and energy storage and the circular economy of polymers.

EXPERIMENTAL SECTION

Materials and General Methods. All air-sensitive reactions were performed under N_2 by means of standard Schlenk or glove box techniques. All metathesis reactions were performed under N_2. Solvents for ring-opening reactions and deuterated solvents for NMR spectroscopy were degassed and filtered through basic alumina before use. Poly(styrene) standards and $Cl_2(H_2IMes)(PCy_3)Ru{=}CHPh$, **7**, were purchased from Aldrich. The synthesis of $(3\text{-Br-Pyr})_2Cl_2(H_2IMes)Ru{=}CHPh$ (**5**) was performed according to the procedure reported by Love et al.[61] Dry, oxygen-free CH_2Cl_2, THF, and DMF were obtained with a Pure Process Technology solvent purification system. Mallinckrodt silica gel-60 (230−400 mesh) was used for column chromatography. Analytical thin-layer chromatography was performed on precoated silica gel plates (60F254), and Combi-Flash chromatography on RediSep normal-phase silica columns (silica gel-60, 230−400 mesh). Bruker Nanobay 400, AVANCE III 500 MHz, and AVANCE III 700 MHz instruments were used for NMR spectroscopy. Chemical shifts (δ, ppm) are relative to the peaks of residual undeuterated solvents: δ 7.28 and 77.22, respectively, for ^{1}H and ^{13}C spectra in $CDCl_3$; δ 1.96 for ^{1}H spectra in d_3-acetonitrile, and δ 118.26 and 1.79 for ^{13}C spectra in d_3-acetonitrile.

Number- and weight-average molecular weights (M_n and M_w) and dispersity indices (D_M) were determined by GPC by using a Phenogel 5 μm 10E4A LC column (300 × 7.8 mm, 5−500 kDa MW), a Phenogel 5 μm linear (2) LC column (300 × 7.8 mm, 100−10,000 kDa MW), and a Phenogel 5 μm, 50 Å LC column (300 × 4.6 nm, 100 Da to 3 kDa MW) with THF as the mobile phase at 30 °C. Output was detected with a Brookhaven Instruments refractive index detector by using an eluent flow rate of 0.7 mL/min and a 100 μL injection loop.

MALDI-TOF mass spectrometry was performed on the Bruker AutoFlex II MALDI-TOF/TOF at mass spectroscopy facility in Chemistry Department, Stony Brook University. Sample preparation: 30 mg 2,5-dihydroxybenzoic acid (DHB) was dissolved in 1 mL of methanol. 5 mg of the polymer was dissolved in 1 mL of methanol. The sample plate was prepared using 5:1 DHB/polymer. 0.4 μL of DHB was added onto the plate + 0.2 μL of polymer + 0.4 μL of DHB.

Thermal analysis was performed on a TA Instruments Q2000 differential scanning calorimeter with Wizard software (TA Instruments Q Series software). Heat flow (Tzero) calibration was performed with sapphire standards, and the temperature (cell constant) was calibrated using indium at a scan rate of 10 °C/min. All discrete scanning calorimetry measurements were performed under a N_2 flow (50 mL/min) using S5 Tzero aluminum pans and hermetic lids. The sample weights ranged from 3 to 8 mg. Polymer samples were first heated from −50 to 200 °C at a rate of 10 °C/min to erase thermal history. The samples were then cooled back to −50 °C at 10 °C/min and reheated to 200 °C at 5 °C/min. The second ramp was used for the thermal analysis of the polymers.

Thermogravimetric analysis was performed with a TA Instruments Q50 Thermogravimetric Analyzer equipped with a platinum pan. The sample sizes ranged from 5 to 15 mg. Weight loss data were collected from 25 to 600 °C at 10 °C/min under a N_2 flow (60 mL/min).

Interfacial Rheology Characterization of Polymers. Interfacial rheological properties of polymer solutions were measured by using a double wall ring (DWR) fixture on a TA Instruments DHR-III rheometer. The DWR trough was loaded with 20 mL of water. The upper DWR fixture was lowered until it made initial contact with the water, as determined by the visual observation of the water surface. Then, 60 μL of a solution containing 1.0 wt % of the copolymer in chloroform was applied dropwise to the surface of the trough. A freshly prepared copolymer solution was used for each run. The solution was allowed to evaporate for 300 s. To ensure the formation of a stable polymer interface, G' and G'' were measured at a stress of 0.1% and a frequency of 1 rad/s as a function of time. Samples typically took 20 min to reach equilibrium. After this time, stress sweeps and frequency sweeps were performed. Before each copolymer system was tested, amplitude sweep tests were performed at a constant frequency, but at variable amplitudes to ensure the frequency sweep tests were performed within the linear viscoelastic regime. All tests were performed at 25 °C.

Preparation of Monomers. *N-Propyl bicyclo[4.2.0]oct-1(8)-ene-8-carboxamide (**1a**).* A modified version of the procedure reported in the literature[43] was used. Specifically, bicyclo[4.2.0]oct-1(8)-ene-8 carboxylic acid (750 mg, 4.93 mmol) and (1-cyano-2-ethoxy-2-oxoethylidenaminooxy)dimethylamino-morpholino-carbenium hexafluorophosphate (2.1 g, 4.93 mmol) were dissolved in 25.0 mL of dimethylformamide, the mixture was purged with N_2 for 15 min, and then *N*,*N*-diisopropylethylamine (1.8 mL, 9.86 mmol) was added. Upon the addition of the amine, the colorless mixture instantly became bright orange. After the mixture was purged with N_2 for an additional 10 min, *N*-propylamine (0.40 mL, 4.93 mmol) was added, and the mixture was stirred vigorously under N2 for 48 h. The resulting dark orange mixture was diluted with 60 mL of CH_2Cl_2, sequentially washed with 1 M HCl (2 × 35 mL), saturated sodium bicarbonate (3 × 45 mL), and distilled water (2 × 45 mL). The organic layer was dried over anhydrous sodium sulfate and filtered, and the filtrate was concentrated in vacuo to afford an off-white solid. Column chromatography (CombiFlash) on silica gel with a solvent gradient of 0−50% ethyl acetate/hexane (R_f = 0.6 in 1:1 ethyl acetate/hexane) afforded **1a** as a white solid (695 mg, 73). The NMR data agreed with the literature data.

*N-Hexyl Bicyclo[4.2.0]oct-1(8)-ene-8-carboxamide (**1b**).* The literature procedure[43] was used.

*Non-6-eno-9-lactone (**2a**).* Monomer **2a** was prepared from but-3-enyl hept-6-enoate by ring-closing metathesis according to the procedure reported by Conrad et al.[44] ^{1}H NMR (700 MHz, $CDCl_3$, δ): 5.82−5.57 (m, 0.1H), 5.58−5.30 (m, 2H), 4.59−4.49 (m, 0.1H), 4.25−3.99 (m, 2H), 2.49−2.37 (m, 0.2H), 2.37−2.17 (m, 4H), 2.05 (m, 2H), 1.79−1.67 (m, 1H), 1.67−1.53 (m, 2H), 1.39 (dt, 2H, J = 14.5, 7.3 Hz), 1.34−1.18 (m, 0.1H).

Prop-2-enyl Hept-6-enoate. In a 2-neck round-bottom flask, 6-heptenoic acid (1 g, 7.80 mmol) and allyl alcohol (0.46 g, 7.93 mmol) were dissolved in 30 mL of dry chloroform, and then *p*-toluenesulfonic acid (1 mol %) was added as the catalyst. The flask was equipped with an inverse Dean−Stark trap that was partially filled with 4 Å molecule sieves and fitted with a condenser. The reaction mixture was heated at reflux with stirring overnight, cooled to room temperature, and washed sequentially with 5% $NaHCO_3$ (3×), 1 N

https://dx.doi.org/10.1021/acs.macromol.0c01051
Macromolecules XXXX, XXX, XXX−XXX

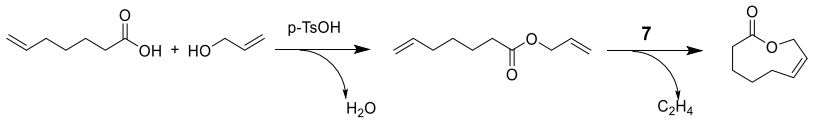

HCl (3×), and brine (2×) to completely remove the *p*-toluenesulfonic acid. The solvent was then removed under reduced pressure. Silica gel column chromatography (5% ethyl acetate in hexane) afforded pure product (1.0 g, 75% isolated yield). ^{1}H NMR (400 MHz, $CDCl_3$, δ): 6.07−5.68 (m, 2H), 5.45−4.85 (m, 4H), 4.66−4.47 (m, 2H), 2.42−2.26 (m, 2H), 2.13−2.01 (m, 2H), 1.75−1.60 (m, 2H), 1.51−1.37 (m, 2H). ^{13}C NMR (176 MHz, $CDCl_3$, δ): 173.33, 138.39, 132.31, 118.11, 114.70, 64.96, 34.08, 33.36, 28.33, 24.39.

*8-Hydroxy-6-octanoic Acid Lactone (**2b**).* A solution of Grubbs 2nd generation catalyst **7** (24 mg, 0.0283 mmol) in 10 mL of CH_2Cl_2 was added all at once to a solution of prop-2-enyl hept-6-enoate (100 mg, 0.595 mmol) in 250 mL of CH_2Cl_2. The resulting solution was stirred at 22 °C for 15 min, heated at reflux for 5 h, and then concentrated to a volume of ∼1 mL. Purification by chromatography on silica gel (5% ethyl acetate in CH_2Cl_2) afforded **2b** as a mixture of 70% cis and 30% trans cis isomers (50.9 mg, 47.6% isolated yield). ^{1}H NMR (400 MHz, $CDCl_3$, δ): 5.93−5.31 (m, 2H), 4.72−4.43 (m, 2H), 2.41−2.22 (m, 2H), 2.14−1.98 (m, 2H), 1.75−1.53 (m, 2H), 1.41 (tt, 2H, J = 9.7, 4.9 Hz). ^{13}C NMR (126 MHz, $CDCl_3$, δ): 173.22, 135.83, 130.41, 127.46, 124.50, 77.32, 77.06, 76.81, 64.59, 63.24, 34.67, 32.04, 31.67, 28.65, 27.67, 24.77, 24.66. MS (+EI) calcd for $C_8H_{12}O_2$ $[M + H]^+$, 141.1; found, 141.1.

*2-Phenyl-4,7-dihydro-1,3-dioxepin (**3b**).* A modified literature procedure[34] was followed. Specifically, benzaldehyde (1.05 g, 9.8 mmol), *cis*-2-butene-1,4-diol (1.1 g, 12.5 mmol), and *p*-toluenesulfonic acid (30 mg, 0.16 mmol) were dissolved in 20 mL of CH_2Cl_2. Enough anhydrous magnesium sulfate was added to clarify the mixture, which was then stirred at room temperature overnight, passed through a basic alumina plug, and microdistilled to afford **3b** as a colorless oil (1.38 g, 80% yield, purity >98% as indicated by ^{1}H NMR spectroscopy). ^{1}H NMR (700 MHz, CDCl3, δ): 7.56 (m, 2H), 7.41 (dd, 2H, J = 8.20, 6.56 Hz), 7.37 (m, 1H), 5.89 (s, 1H), 5.80 (d, 2H, J = 1.83 Hz), 4.43 (dt, 2H, J = 16.2, 2.47 Hz), 4.31 (dt, 2H, J = 16.4, 2.21 Hz). ^{13}C NMR (700 MHz, CDCl3, δ): 139.0, 130.1, 128.6, 128.4, 126.6, 102.3, 64.7. These data agree with the literature data.[34]

*2-Methyl-4,7-dihydro-1,3-dioxepin (**3c**).* A modified literature procedure[34] was followed. Acetaldehyde (1.57 g, 35.6 mmol), *cis*-2-butene-1,4-diol (3.00 g, 34.1 mmol), and *p*-toluenesulfonic acid (52 mg, 0.27 mmol) were dissolved in 40 mL of 1:4 THF/CH_2Cl_2. Enough anhydrous magnesium sulfate was added to clarify the mixture, which was then stirred at room temperature overnight, passed through a short alumina plug, concentrated, and was distilled via the microdistillation setup to afford **3c** as an oil (3.1 g, 80%, purity >95% as indicated by 1H NMR spectroscopy). ^{1}H NMR (700 MHz, CDCl3, δ): 5.75 (d, 2H, J = 1.8 Hz), 5.03 (q, 1H, J = 5.2 Hz), 4.41 (dt, 2H, J = 16.2, 2.50 Hz), 4.20 (dt, 2H, J = 16.2, 2.22 Hz), 1.38 (d, 3H, J = 5.2 Hz). ^{13}C NMR (700 MHz, CDCl3, δ): 150.0, 101.3, 64.9, 20.2. These data agree with the literature data.[34]

*(1R,2S,4R)-N-Hexylbicyclo[2.2.1]hept-5-ene-2-carboxamide (**4**).* *exo*-5-Norbornenecarboxylic acid (300 mg, 2.17 mmol) and (1-cyano-2-ethoxy-2-oxoethylidenaminooxy)dimethylamino-morpholino-carbenium hexafluorophosphate (930 mg, 2.17 mmol) were dissolved in 20 mL of dimethylformamide followed by the addition of *N*-hexylamine (284 μL, 2.17 mmol). The procedure used to synthesize **1a** afforded **4** (445 mg, 93%).[43] ^{1}H NMR (500 MHz, CDCl3, δ): 6.15−6.11 (dd, 2H, J = 15.4, 2.90 Hz), 5.51 (s, 1H), 3.27 (m, 2H), 2.92 (s, 2H), 1.95 (m, 2H), 1.74 (d, 1H, J = 8.23 Hz), 1.51 (p, 2H, J = 7.23, 2.17 Hz), 1.33 (m, 8H), 0.89 (m, 3H). ^{13}C NMR (500 MHz, CDCl3, δ): 175.7, 138.2, 136.2, 47.4, 46.6, 44.9, 41.8, 39.9, 31.8, 30.7, 29.9, 26.8, 22.8, 14.2. ESI-MS m/z calcd, 222.2; found, 222.1 $[M + H]^+$.

Preparation of Polymers. *General Procedure for AROMP Polymers.* Reaction vessels and reagents were maintained under oxygen-free conditions. For preliminary experiments, an NMR tube capped with a PTFE-lined septum was charged with a solution of catalyst **5** (1 mg per 80 μL of $CDCl_3$). Then, a solution of 1 (10 mg per 10 μL of $CDCl_3$) was added, and the reaction mixture was incubated at 40 °C with monitoring by ^{1}H NMR. When the monomer was fully initiated (usually 10−15 min), as indicated by the complete disappearance of the ruthenium alkylidene proton at ∼19 ppm, monomer **2** or **3** was added. Upon completion of the reaction (in the case of near 100% conversion, the cyclohexyl proton at ∼2.9 ppm disappeared) or when monomer consumption ceased, the reaction was quenched with excess ethyl vinyl ether (at least 500-fold with respected to **5**) and stirred for 20 min. Polymers synthesized with monomer **2** were purified through precipitation in cold diethyl ether at least three times. Polymers synthesized with monomer **3** were purified by precipitation with hexanes at least three times. The precipitates were vacuum-dried.

*Poly(**1a**-alt-**2a**)$_{10}$.* Amide **1a** (24.5 mg, 127.6 μmol), catalyst **5** (11.3 mg, 12.8 μmol), and **2a** (19.7 mg, 127.6 μmol) were mixed in $CDCl_3$ in an NMR tube. After 5 h, amide **1a** was completely consumed. Precipitation in cold diethyl ether yielded poly(**1a**-*alt*-**2a**)$_{10}$. ^{1}H NMR (500 MHz, $CDCl_3$, δ): 6.28−6.04 (m, 9H), 6.03−5.59 (m, 9H), 5.42−5.20 (m, 1H), 5.04 (m, 8H), 4.72−4.55 (m, 3H), 4.31−3.88 (m, 20H), 3.36−3.12 (m, 20H), 2.69−1.91 (m, 112H), 1.81−1.20 (m, 127H), 0.94 (t, 30H, J = 7.3 Hz). $M_{n,theo}$ = 3.5 kDa, $M_{n,meas}$ = 4.8 kDa, $M_{w,meas}$ = 7.4 kDa, $Đ_M$ = 1.5.

*Poly(**1a**-alt-**2a**)$_{50}$.* Amide **1a** (24.5 mg, 127.6 μmol), catalyst **5** (2.2 mg, 2.6 μmol, 1 equiv), and **2a** (19.7 mg, 127.6 μmol) were mixed in $CDCl_3$ in an NMR tube. After 18 h, amide **1a** was completely consumed. Precipitation in cold diethyl ether yielded poly(**1a**-*alt*-**2a**)$_{50}$. ^{1}H NMR (500 MHz, $CDCl_3$, δ): 6.21−6.03 (m, 45H), 5.99−5.56 (m, 55H), 5.15 (d, 50H, J = 110.5 Hz), 4.21−4.05 (m, 100H), 3.39−3.16 (m, 100H), 2.66−1.94 (m, 550H), 1.89−1.25 (m, 650H), 0.95 (t, J = 7.3 Hz, 150H). $M_{n,theo}$ = 17.3 kDa, $M_{n,meas}$ = 20.8 kDa, $M_{w,meas}$ = 27.7 kDa, $Đ_M$ = 1.3.

*Poly(**1a**-alt-**2b**)$_{10}$.* Amide **1a** (24.5 mg, 127.6 μmol), catalyst **5** (11.3 mg, 12.8 μmol), and **2b** (17.9 mg, 127.6 μmol) were mixed in $CDCl_3$ in an NMR tube. After 5 h, amide **1a** was completely consumed. Precipitation in cold diethyl ether yielded poly(**1a**-*alt*-**2b**)$_{10}$. ^{1}H NMR (700 MHz, $CDCl_3$, δ): 6.28−6.05 (m, 10H), 6.06−5.58 (m, 8H), 5.56−5.31 (m, 1H), 5.22 (m, 6H), 5.00 (s, mH), 4.78−4.48 (m, 20H), 3.37−3.13 (m, 20H), 2.78−2.49 (m, 12H), 2.49−1.80 (m, 92H), 1.77−1.07 (m, 128H), 0.93 (t, 30H, J = 7.0 Hz). $M_{n,theo}$ = 3.3 kDa, $M_{n,meas}$ = 5.1 kDa, $M_{w,meas}$ = 7.6 kDa, $Đ_M$ = 1.5.

*Poly(**1a**-alt-**2b**)$_{50}$.* Amide **1a** (24.5 mg, 127.6 μmol), catalyst **5** (2.2 mg, 2.6 μmol), and **2b** (17.9 mg, 127.6 μmol) were mixed in $CDCl_3$ in an NMR tube. After 18 h, amide **1a** was completely consumed. Precipitation in cold diethyl ether yielded poly(**1a**-*alt*-**2b**)$_{50}$. ^{1}H NMR (700 MHz, $CDCl_3$, δ): 6.26−6.00 (m, 51H), 6.00−5.29 (m, 40H), 5.23 (m, 30H), 5.01 (m, 15H), 4.76−4.46 (m, 100H), 3.34−3.14 (m, 100H), 2.73−1.86 (m, 460H), 1.84−1.09 (m, 610H), 1.02−0.86 (m, 150H). $M_{n,theo}$ = 16.6 kDa, $M_{n,meas}$ = 12.8 kDa, $M_{w,meas}$ = 20.2 kDa, $Đ_M$ = 1.6.

*Poly(**1b**-alt-**2a**)$_{10}$.* Amide **1b** (30.0 mg, 127.6 μmol), catalyst **5** (11.3 mg, 12.8 μmol), and **2a** (19.7 mg, 127.6 μmol) were mixed in $CDCl_3$ in an NMR tube. After 8 h, amide A was completely consumed. Precipitation in cold diethyl ether yielded poly(**1b**-*alt*-**2a**)$_{10}$. ^{1}H NMR (700 MHz, $CDCl_3$, δ): 6.19−5.99 (m, 6H), 5.95−5.59 (m, 1H), 5.58−5.45 (m, 4H), 5.45−5.32 (m, 3H), 5.12−4.93 (m, 6H), 4.18−3.98 (m, 20H), 3.41−3.15 (m, 20H), 2.69−1.87 (m, 120H), 1.76−1.17 (m, 196H), 0.94−0.88 (m, 30H). $M_{n,theo}$ = 3.9 kDa, $M_{n,meas}$ = 4.3 kDa, $M_{w,meas}$ = 6.6 kDa, $Đ_M$ = 1.5.

*Poly(**1b**-alt-**2b**)$_{10}$.* Amide **1b** (30 mg, 127.6 μmol), catalyst **5** (11.3 mg, 12.8 μmol), and **2b** (17.9 mg, 127.6 μmol) were mixed in $CDCl_3$ in an NMR tube. After 8 h, amide **1b** was completely consumed. Precipitation in cold diethyl ether yielded poly(**1b**-*alt*-**2b**)$_{10}$. ^{1}H NMR (400 MHz, $CDCl_3$, δ): 6.20−5.95 (m, 9H), 5.95−5.30 (m, 6H),

https://dx.doi.org/10.1021/acs.macromol.0c01051
Macromolecules XXXX, XXX, XXX−XXX

5.31−5.11 (m, 6H), 5.11−4.89 (m, 3H), 4.72−4.48 (m, 16H), 3.45−3.05 (m, 20H), 2.88−1.90 (m, 103H), 1.76−1.21 (m, 188H), 0.91−0.83 (m, 30H). $M_{n,theo}$ = 3.8 kDa, $M_{n,meas}$ = 6.0 kDa, $M_{w,meas}$ = 9.8 kDa, $Đ_M$ = 1.6.

*Poly(**1b**-alt-**2b**)$_{50}$.* Amide **1b** (30 mg, 127.6 μmol), catalyst **5** (2.2 mg, 2.6 μmol), and **2b** (17.9 mg, 127.6 μmol) were mixed in $CDCl_3$ in an NMR tube. After 21 h, amide **1b** was completely consumed. Precipitation in cold diethyl ether yielded poly(**1b**-*alt*-**2b**)$_{50}$. ^{1}H NMR (400 MHz, $CDCl_3$, δ): 6.19−6.00 (m, 41H), 6.00−5.30 (m, 54H), 5.22 (t, 26H, *J* = 6.1 Hz), 5.00 (t, 13H, *J* = 6.7 Hz), 4.75−4.39 (m, 88H), 3.38−3.12 (m, 100H), 2.68−1.83 (m, 475H), 1.80−0.90 (m, 956H), 0.89−0.82 (m, 154H). $M_{n,theo}$ = 15.2 kDa, $M_{n,meas}$ = 14.2 kDa, $M_{w,meas}$ = 19.6 kDa, $Đ_M$ = 1.4.

*Poly(**1a**-alt-**3a**)$_m$ (m = 20, 50, and 100).* For the preparation of the 20-mer, a 4 mL vial equipped with a PTFE-lined cap and a stir bar was charged with 550 μL of a solution of **5** in chloroform (6.9 mg, 7.8 μmol), and then 300 μL of monomer **1a** solution in chloroform (30 mg, 155 μmol) was added all at once. After initiation at 40 °C for 15 min, monomer **3a** (16 μL, 16 mg, 155 μmol) was added to the hot reaction mixture and stirring was continued for an additional 2 h. The mixture was then cooled to rt and quenched with excess ethyl vinyl ether, and the polymer was precipitated with hexanes (three times) and vacuum-dried to give a reddish-brown solid in 70% isolated yield. For the preparation of the 50- and 100-mers, the [**5**]/[**1a**]/[**3a**] ratios were 1:50:50 and 1:100:100, respectively. Selected NMR data for the signature region of poly(**1a**-*alt*-**3a**)$_m$: ^{1}H NMR (500 MHz, $CDCl_3$, δ): 6.18 (t, 1H, *J* = 6.02 Hz), 5.98 (br, 1H), 5.26 (t, 1H, *J* = 6.77 Hz), 4.69 (s, 2H), 4.19 (d, 2H, *J* = 5.89 Hz), 4.08 (m, 2H), 3.26 (dq, 2H, *J* = 15.2 Hz, 7.71, 7.30). ^{13}C NMR (500 MHz, $CDCl_3$, δ): 169.7 (CONHR), 147.6, 139.4, 130.3, 117.0, 94.3, 93.8, 64.1, 63.5.

*Poly(**1a**-alt-**3b**)$_m$ (m = 20, 50, and 100).* For the preparation of the 20-mer, a 4 mL vial equipped with a PTFE-lined cap and a stir bar was charged with 650 μL of a solution of **5** in chloroform (8 mg, 9.1 μmol), and then 350 μL of monomer **1a** solution in chloroform (35 mg, 181 μmol) was added. After initiation at 40 °C for 15 min, monomer **3b** (57 μL, 64 mg, 363 μmol) was added to the hot reaction mixture and stirring was continued for an additional 3 h. The mixture was then cooled to rt before quenching with excess ethyl vinyl ether, and the polymer was precipitated with hexanes and vacuum-dried to yield a dark yellowish-brown solid in 75% isolated yield. For the preparation of the 50- and 100-mers, the [**5**]/[**1a**]/[**3b**] ratios were 1:50:100 and 1:100:200, respectively. Selected NMR data for the signature region of poly(**1a**-*alt*-**3b**)$_m$: ^{1}H NMR (500 MHz, $CDCl_3$, δ): 7.46 (m, 2H), 7.35 (dt, 3H, *J* = 15.9, 8.93 Hz), 6.16 (t, 1H, *J* = 6.31 Hz), 5.90 (br s, 1H), 5.55 (1H, s), 5.22 (t, 1H, *J* values not determined), 4.11 (m, 4H), 3.19 (t, 2H, *J* values not determined). ^{13}C NMR (500 MHz, $CDCl_3$, δ): 169.7, 146.9, 139.1, 138.5, 130.4, 128.8, 128.5, 126.9, 117.3, 100.9, 61.7.

*Poly(**1a**-alt-**3c**)$_m$ (m = 20, 50).* For the preparation of the 20-mer, a 4 mL vial equipped with a PTFE-lined cap and a stir bar was charged with 650 μL of a solution of **5** in chloroform (11.5 mg, 13.0 μmol), and then 350 μL of monomer **1a** solution in chloroform (50 mg, 260 μmol) was added. After initiation at 40 °C for 15 min, monomer **3c** (28 μL, 30 mg, 260 μmol) was added to the hot reaction mixture and stirring was continued for an additional 2 h. The mixture was then cooled to room temperature before quenching with excess ethyl vinyl ether, and the polymer was precipitated with hexanes and vacuum-dried to yield a dark yellowish-brown solid in 80% isolated yield. Selected NMR data for the signature region of poly(**1a**-*alt*-**3c**)$_{20}$: ^{1}H NMR (700 MHz, $CDCl_3$, δ): 6.18 (d, 1H, *J* = 5.67 Hz), 5.24 (t, 1H, *J* = 6.81 Hz), 4.70 (q, 1H, *J* = 5.89 Hz) 4.11 (m, 4H), 3.25 (m, 2H). ^{13}C NMR (700 MHz, $CDCl_3$, δ): 169.7, 146.4, 138.9, 130.7, 129.0, 128.6, 117.6, 99.1, 61.4. For 50 mer, the [**5**]/[**1a**]/[**3c**] ratios were 1:50:90. Selected NMR data for the signature region of poly(**1a**-*alt*-**3c**)$_{50}$: ^{1}H NMR (700 MHz, DMSO-d_6, δ): 7.90 (s, 1H, CONHR), 6.13 (d, 1H, *J* = 5.81 Hz), 5.14 (t, 1H, *J* = 6.78 Hz), 4.69 (m, 1H) 4.05 (m, 4H), 3.03 (m, 2H). ^{13}C NMR (700 MHz, DMSO-d_6, δ): 168.8, 145.5, 137.9, 130.8, 129.9, 129.0, 117.8, 98.7, 61.6.

*Poly(**4**)$_{20}$-b-poly(**1a**-alt-**3a**)$_{12}$.* A 4 mL vial equipped with a PTFE-lined cap and a stir bar was charged with 320 μL of the solution of **5** in methylene chloride (10 mg, 11 μmol) and chilled at 0 °C, and then 87 μL of monomer **4** solution (50 mg, 230 μmol) was added all at once. After initiation for 5 min at 0 °C and then for 25 min at room temperature, a 100 μL of aliquot was removed and quenched with ethyl vinyl ether (100 μL); subsequent precipitation with diethyl ether (3×) yielded poly(**4**)$_{20}$ as an off-white solid. To the remaining mixture in the vial (which contained approximately 8.8 μmol of poly(**4**)$_{20}$-appended catalyst), 260 μL of **1a** solution in CH_2Cl_2 (42.2 mg, 220 μmol) and **3a** (21 μL, 22 mg, 220 μmol) were added in that order. The mixture was incubated at 40 °C for 2 h and quenched with ethyl vinyl ether (50 μL); precipitation with diethyl ether (3×) yielded the diblock copolymer as an off-white solid. The polymer was vacuum-dried overnight prior to use.

*Poly(**4**)$_{20}$-b-poly(**1a**-alt-**3b**)$_{10}$.* A 4 mL vial was charged with 400 μL of the solution of **5** in methylene chloride (10.8 mg, 12.2 μmol), and then 180 μL of monomer **4** solution in CH_2Cl_2 (53 mg, 240 μmol) was added all at once. Reaction went for 25 min at rt, a 150 μL of aliquot was removed and quenched with ethyl vinyl ether (100 μL); precipitation with diethyl ether (3×) yielded poly(**4**)$_{20}$ as an off-white solid. To the remaining mixture in the vial (which contained approximately 8.8 μmol of poly(**4**)$_{20}$-appended catalyst), 350 μL of **1a** solution in methylene chloride (42.7 mg, 220 μmol) and **3b** (71 μL, 78 mg, 440 μmol) in that order. The mixture was incubated at 40 °C for 19 h and quenched with ethyl vinyl ether (50 μL); precipitation with diethyl ether (3×) yielded the diblock copolymer as an off-white solid. The polymer was vacuum-dried overnight prior to use.

*Poly(**4**)$_{20}$-b-poly(**1a**-alt-**3c**)$_{10}$.* A 4 mL vial was charged with 200 μL of the solution of **5** in CH_2Cl_2 (7.9 mg, 9.00 μmol) and chilled at 0 °C, and then 300 μL of monomer **4** solution (40 mg, 179 μmol) was added quickly. After initiation for 5 min at 0 °C and warming to room temperature over the course of 25 min, a 150 μL of aliquot was removed and quenched with ethyl vinyl ether (50 μL); precipitation with diethyl ether (3×) yielded poly(**4**)$_{20}$ as an off-white solid. To the remaining mixture in the vial (containing approximately 6.3 μmol of poly(**4**)$_{20}$-appended catalyst), 260 μL of **1a** solution (30.4 mg, 158 μmol) was added followed by **3c** (17 μL, 158 μmol). The mixture was incubated at 40 °C for 3 h and quenched with ethyl vinyl ether (50 μL); precipitation with diethyl ether (3×) yielded the diblock copolymer as an off-white solid. The polymer was vacuum-dried overnight prior to use.

*Hydrolysis of Poly(**1**-alt-**2b**)$_{10}$.* Poly(**1a**-*alt*-**2b**)$_{10}$ (3 mg) and poly(**1b**-*alt*-**2b**)$_{10}$ (3 mg) were each dissolved separately in 1:1 acetonitrile/CH_2Cl_2 (300 μL each), owing to the limited solubility of these copolymers in water. Each solution was then treated with 1 mL of 0.1 M NaOH at 40 °C with stirring. Degradation was monitored by means of ^{1}H NMR spectroscopy with tetramethylsilane as an internal standard. The degradation products were purified by HPLC with 0.1% formic acid in water as the aqueous solvent and acetonitrile as the organic solvent (Luna 5 μm C18(2) 100 Å, LC Column 250 × 10 mm) Eluates were collected and tested using Mass Spec to identify the structures of degraded polymer fragments. M = 351.2, found $[M + Na]^+$. Samples of polymer solution were also treated with citric acid−Na_2HPO_4 buffer solutions at pH = 2.6, 5.0, 7.4, and Na_2CO_3−$NaHCO_3$ buffer solutions at pH = 10.8 at 40 °C with stirring but no significant degradation was seen after 5 days, which was expected as polyesters were known to degrade slowly.[62]

*Kinetics of Poly(**1a**-alt-**3a**/**3b**)$_{20}$ Hydrolysis.* Polymer (5 mg, 1.4 μmol) was dissolved in 500 μL of d_3-acetonitrile, and the solution was transferred to an NMR tube with a PTFE-lined cap. Then, 250 μL of 0.2 M sodium phosphate buffer (in D_2O, pH 5) was added. The reaction mixture was incubated at 37 °C, and the reaction progress was monitored by ^{1}H NMR. In the case of poly(**1a**-*alt*-**3a**)$_{20}$, hexylamine was added as a scavenging agent of formaldehyde.

Hydrolysis of poly(**4**)$_{20}$-*b*-poly(**1a**-*alt*-**3**)$_m$ at pH 1. Each polymer (30 mg) was added to 1 mL of THF in a 4 mL vial capped with a PTFE-lined septum, and then 0.3 mL of 10 mM aqueous TFA was added. For poly(**4**)$_{20}$-*b*-poly(**1a**-*alt*-**3a**)$_m$, *N*-hexylamine (15 μL, 114 μmol) was added to scavenge-evolved formaldehyde. The hydrolysis reaction was carried out at 37 °C, and aliquots were periodically removed for analysis. Polymers were precipitated with diethyl ether

https://dx.doi.org/10.1021/acs.macromol.0c01051
Macromolecules XXXX, XXX, XXX−XXX

and vacuum dried. The average molecular weights of the residual polymers were acquired by GPC.

Hydrolysis of poly(**4**)$_{20}$-*b*-poly(**1a**-*alt*-**3**)$_m$ at pH 5. Each polymer was dissolved in 1.0 mL of THF, and then 0.25 mL of 0.2 M sodium phosphate buffer (pH 5) was added. The mixture was incubated at 37 °C, and aliquots were removed periodically for analysis. Polymers were precipitated from diethyl ether and analyzed by GPC.

■ ASSOCIATED CONTENT

Supporting Information

The Supporting Information is available free of charge at https://pubs.acs.org/doi/10.1021/acs.macromol.0c01051.

Reaction kinetic data, experimental details for strain amplitude sweep, time-dependent modulus plots, and spectral characterizations data (PDF)

■ AUTHOR INFORMATION

Corresponding Author

Nicole S. Sampson − *Department of Chemistry, Stony Brook University, Stony Brook, New York 11794-3400, United States;* orcid.org/0000-0002-2835-7760; Email: nicole.sampson@stonybrook.edu

Authors

Francis O. Boadi − *Department of Chemistry, Stony Brook University, Stony Brook, New York 11794-3400, United States;* orcid.org/0000-0002-2064-5151

Jingling Zhang − *Department of Materials Science and Chemical Engineering, Stony Brook University, Stony Brook, New York 11794-2275, United States;* orcid.org/0000-0002-5595-0666

Xiaoxi Yu − *Department of Chemistry, Stony Brook University, Stony Brook, New York 11794-3400, United States*

Surita R. Bhatia − *Department of Chemistry, Stony Brook University, Stony Brook, New York 11794-3400, United States;* orcid.org/0000-0002-5950-193X

Complete contact information is available at: https://pubs.acs.org/10.1021/acs.macromol.0c01051

Notes

The authors declare no competing financial interest.

■ ACKNOWLEDGMENTS

This research is funded by the NSF CHE1609494 (N.S.S.), the NIH R01GM097971 (N.S.S.), the NIH T32GM092714 (F.O.B.), the ACS PRF 55729-ND9 (S.R.B.), and the DOE Contract DE-SC0012704 (the CFN at the Brookhaven National Laboratory). Shearson Editorial Services (Cornwall, NY, U.S.A.) provided English language editing of the text of this paper.

■ REFERENCES

(1) Langer, R.; Vacanti, J. Tissue Engineering. *Science* **1993**, *260*, 920−926.

(2) Dvir, T.; Timko, B. P.; Kohane, D. S.; Langer, R. Nanotechnological Strategies for Engineering Complex Tissues. *Nat. Nanotechnol.* **2011**, *6*, 13−22.

(3) Liu, B.; Thayumanavan, S. Substituent Effects on the pH Sensitivity of Acetals and Ketals and Their Correlation with Encapsulation Stability in Polymeric Nanogels. *J. Am. Chem. Soc.* **2017**, *139*, 2306−2317.

(4) Song, R.; Murphy, M.; Li, C.; Ting, K.; Soo, C.; Zheng, Z. Current Development of Biodegradable Polymeric Materials for Biomedical Applications. *Drug Des., Dev. Ther.* **2018**, *12*, 3117−3145.

(5) Ober, M. S.; Romer, D. R.; Etienne, J.; Thomas, P. J.; Jain, V.; Cameron, J. F.; Thackeray, J. W. Backbone Degradable Poly(Aryl Acetal) Photoresist Polymers: Synthesis, Acid Sensitivity, and Extreme Ultraviolet Lithography Performance. *Macromolecules* **2019**, *52*, 886−895.

(6) Cushen, J. D.; Bates, C. M.; Rausch, E. L.; Dean, L. M.; Zhou, S. X.; Willson, C. G.; Ellison, C. J. Thin Film Self-Assembly of Poly(Trimethylsilylstyrene-B-D,L-Lactide) with Sub-10 nm Domains. *Macromolecules* **2012**, *45*, 8722−8728.

(7) Pal, R. K.; Kundu, S. C.; Yadavalli, V. K. Fabrication of Flexible, Fully Organic, Degradable Energy Storage Devices Using Silk Proteins. *ACS Appl. Mater. Interfaces* **2018**, *10*, 9620−9628.

(8) Gao, M.; Shih, C.-C.; Pan, S.-Y.; Chueh, C.-C.; Chen, W.-C. Advances and Challenges of Green Materials for Electronics and Energy Storage Applications: From Design to End-of-Life Recovery. *J. Mater. Chem. A* **2018**, *6*, 20546−20563.

(9) Feig, V. R.; Tran, H.; Bao, Z. Biodegradable Polymeric Materials in Degradable Electronic Devices. *ACS Cent. Sci.* **2018**, *4*, 337−348.

(10) Hufendiek, A.; Lingier, S.; Du Prez, F. E. Thermoplastic Polyacetals: Chemistry from the Past for a Sustainable Future? *Polym. Chem.* **2019**, *10*, 9−33.

(11) Winnacker, M.; Rieger, B. Poly(Ester Amide)S: Recent Insights into Synthesis, Stability and Biomedical Applications. *Polym. Chem.* **2016**, *7*, 7039−7046.

(12) Stukenbroeker, T. S.; Bandar, J. S.; Zhang, X.; Lambert, T. H.; Waymouth, R. M. Cyclopropenimine Superbases: Competitive Initiation Processes in Lactide Polymerization. *ACS Macro Lett.* **2015**, *4*, 853−856.

(13) Ishido, Y.; Aburaki, R.; Kanaoka, S.; Aoshima, S. Well-Defined Alternating Copolymers of Benzaldehydes with Vinyl Ethers: Precision Synthesis by Cationic Copolymerization and Quantitative Degradation to Cinnamaldehydes. *Macromolecules* **2010**, *43*, 3141−3144.

(14) Yokota, D.; Kanazawa, A.; Aoshima, S. Alternating Degradable Copolymers of an Ionic Liquid-Type Vinyl Ether and a Conjugated Aldehyde: Precise Synthesis by Living Cationic Copolymerization and Dual Rare Thermosensitive Behavior in Solution. *Macromolecules* **2019**, *52*, 6241−6249.

(15) Ouchi, M.; Terashima, T.; Sawamoto, M. Transition Metal-Catalyzed Living Radical Polymerization: Toward Perfection in Catalysis and Precision Polymer Synthesis. *Chem. Rev.* **2009**, *109*, 4963−5050.

(16) Bielawski, C. W.; Grubbs, R. H. Living Ring-Opening Metathesis Polymerization. *Prog. Polym. Sci.* **2007**, *32*, 1−29.

(17) Gilliom, L. R.; Grubbs, R. H. Titanacyclobutanes Derived from Strained, Cyclic Olefins: The Living Polymerization of Norbornene. *J. Am. Chem. Soc.* **1986**, *108*, 733−742.

(18) Schrock, R. R. Living Ring-Opening Metathesis Polymerization Catalyzed by Well-Characterized Transition-Metal Alkylidene Complexes. *Acc. Chem. Res.* **1990**, *23*, 158−165.

(19) Matyjaszewski, K. Ranking Living Systems. *Macromolecules* **1993**, *26*, 1787−1788.

(20) Coca, S.; Paik, H.-j.; Matyjaszewski, K. Block Copolymers by Transformation of Living Ring-Opening Metathesis Polymerization into Controlled/"Living" Atom Transfer Radical Polymerization. *Macromolecules* **1997**, *30*, 6513−6516.

(21) Nomura, K.; Abdellatif, M. M. Precise Synthesis of Polymers Containing Functional End Groups by Living Ring-Opening Metathesis Polymerization (Romp): Efficient Tools for Synthesis of Block/Graft Copolymers. *Polymer* **2010**, *51*, 1861−1881.

(22) Fishman, J. M.; Kiessling, L. L. Synthesis of Functionalizable and Degradable Polymers by Ring-Opening Metathesis Polymerization. *Angew. Chem., Int. Ed.* **2013**, *52*, 5061−5064.

(23) Gutekunst, W. R.; Hawker, C. J. A General Approach to Sequence-Controlled Polymers Using Macrocyclic Ring Opening Metathesis Polymerization. *J. Am. Chem. Soc.* **2015**, *137*, 8038−8041.

(24) Mallick, A.; Xu, Y.; Lin, Y.; He, J.; Chan-Park, M. B.; Liu, X.-W. Oxadiazabicyclooctenone as a Versatile Monomer for the Con-

struction of Ph Sensitive Functional Polymers Via Romp. *Polym. Chem.* **2018**, *9*, 372−377.
(25) Nowalk, J. A.; Fang, C.; Short, A. L.; Weiss, R. M.; Swisher, J. H.; Liu, P.; Meyer, T. Y. Sequence-Controlled Polymers through Entropy-Driven Ring-Opening Metathesis Polymerization: Theory, Molecular Weight Control, and Monomer Design. *J. Am. Chem. Soc.* **2019**, *141*, 5741−5752.
(26) Bhaumik, A.; Peterson, G. I.; Kang, C.; Choi, T.-L. Controlled Living Cascade Polymerization to Make Fully Degradable Sugar-Based Polymers from D-Glucose and D-Galactose. *J. Am. Chem. Soc.* **2019**, *141*, 12207−12211.
(27) Feist, J. D.; Xia, Y. Enol Ethers Are Effective Monomers for Ring-Opening Metathesis Polymerization: Synthesis of Degradable and Depolymerizable Poly(2,3-Dihydrofuran). *J. Am. Chem. Soc.* **2020**, *142*, 1186−1189.
(28) Fu, L.; Sui, X.; Crolais, A. E.; Gutekunst, W. R. Modular Approach to Degradable Acetal Polymers Using Cascade Enyne Metathesis Polymerization. *Angew. Chem., Int. Ed.* **2019**, *58*, 15726−15730.
(29) Chang, C.-C.; Emrick, T. Functional Polyolefins Containing Disulfide and Phosphoester Groups: Synthesis and Orthogonal Degradation. *Macromolecules* **2014**, *47*, 1344−1350.
(30) Shieh, P.; Nguyen, H. V.-T.; Johnson, J. A. Tailored Silyl Ether Monomers Enable Backbone-Degradable Polynorbornene-Based Linear, Bottlebrush and Star Copolymers through Romp. *Nat. Chem.* **2019**, *11*, 1124−1132.
(31) Fraser, C.; Hillmyer, M. A.; Gutierrez, E.; Grubbs, R. H. Degradable Cyclooctadiene/Acetal Copolymers: Versatile Precursors to 1,4-Hydroxytelechelic Polybutadiene and Hydroxytelechelic Polyethylene. *Macromolecules* **1995**, *28*, 7256−7261.
(32) Hilf, S.; Grubbs, R. H.; Kilbinger, A. F. M. Sacrificial Synthesis of Hydroxy-Functionalized Romp Polymers: An Efficiency Study. *Macromolecules* **2008**, *41*, 6006−6011.
(33) Hilf, S.; Kilbinger, A. F. M. Thiol-Functionalized Romp Polymers Via Sacrificial Synthesis. *Macromolecules* **2009**, *42*, 4127−4133.
(34) Moatsou, D.; Nagarkar, A.; Kilbinger, A. F. M.; O'Reilly, R. K. Degradable Precision Polynorbornenes Via Ring-Opening Metathesis Polymerization. *J. Polym. Sci., Part A: Polym. Chem.* **2016**, *54*, 1236−1242.
(35) Hilf, S.; Kilbinger, A. F. M. Sacrificial Synthesis of Hydroxy-Telechelic Metathesis Polymers Via Multiblock-Copolymers. *Macromolecules* **2009**, *42*, 1099−1106.
(36) Hilf, S.; Berger-Nicoletti, E.; Grubbs, R. H.; Kilbinger, A. F. M. Monofunctional Metathesis Polymers Via Sacrificial Diblock Copolymers. *Angew. Chem., Int. Ed.* **2006**, *45*, 8045−8048.
(37) Perrier, S.; Wang, X. Sacrificial Synthesis. *Nature* **2007**, *445*, 271−272.
(38) Tan, L.; Li, G.; Parker, K. A.; Sampson, N. S. Ru-Catalyzed Isomerization Provides Access to Alternating Copolymers Via Ring-Opening Metathesis Polymerization. *Macromolecules* **2015**, *48*, 4793−4800.
(39) Elling, B. R.; Xia, Y. Living Alternating Ring-Opening Metathesis Polymerization Based on Single Monomer Additions. *J. Am. Chem. Soc.* **2015**, *137*, 9922−9926.
(40) Zhang, J.; Li, G.; Sampson, N. S. Incorporation of Large Cycloalkene Rings into Alternating Copolymers Allows Control of Glass Transition and Hydrophobicity. *ACS Macro Lett.* **2018**, *7*, 1068−1072.
(41) Elling, B. R.; Su, J. K.; Xia, Y. Degradable Polyacetals/Ketals from Alternating Ring-Opening Metathesis Polymerization. *ACS Macro Lett.* **2020**, *9*, 180−184.
(42) Li, G.; Sampson, N. S. Alternating Ring-Opening Metathesis Polymerization (Aromp) of Hydrophobic and Hydrophilic Monomers Provides Oligomers with Side-Chain Sequence Control. *Macromolecules* **2018**, *51*, 3932−3940.
(43) Chen, L.; Li, L.; Sampson, N. S. Access to Bicyclo[4.2.0]Octene Monomers to Explore the Scope of Alternating Ring-Opening Metathesis Polymerization. *J. Org. Chem.* **2018**, *83*, 2892−2897.
(44) Conrad, J. C.; Eelman, M. D.; Silva, J. A. D.; Monfette, S.; Parnas, H. H.; Snelgrove, J. L.; Fogg, D. E. Oligomers as Intermediates in Ring-Closing Metathesis. *J. Am. Chem. Soc.* **2007**, *129*, 1024−1025.
(45) M, S. A.; Jaganathan, M.; Dhathathreyan, A. Relevance of Interfacial Viscoelasticity in Stability and Conformation of Biomolecular Organizates at Air/Fluid Interface. *Adv. Colloid Interface Sci.* **2016**, *234*, 80−88.
(46) Hong, S. H.; Wenzel, A. G.; Salguero, T. T.; Day, M. W.; Grubbs, R. H. Decomposition of Ruthenium Olefin Metathesis Catalysts. *J. Am. Chem. Soc.* **2007**, *129*, 7961−7968.
(47) Gianni, M. H.; Adams, M.; Kuivila, H. G.; Wursthorn, K. Conformational Analysis of 1,3-Dioxacyclohept-5-Enes. Proton and Carbon-13 Magnetic Resonance. Evidence for a Twist-Boat Conformation. *J. Org. Chem.* **1975**, *40*, 450−453.
(48) Sarotti, A. M.; Fernández, I.; Spanevello, R. A.; Sierra, M. A.; Suárez, A. G. Π-Stacking Effect on Levoglucosenone Derived Internal Chiral Auxiliaries. A Case of Complete Enantioselectivity Inversion on the Diels−Alder Reaction. *Org. Lett.* **2008**, *10*, 3389−3392.
(49) Hong, S. H.; Sanders, D. P.; Lee, C. W.; Grubbs, R. H. Prevention of Undesirable Isomerization During Olefin Metathesis. *J. Am. Chem. Soc.* **2005**, *127*, 17160−17161.
(50) Engelke, J.; Brandt, J.; Barner-Kowollik, C.; Lederer, A. Strengths and Limitations of Size Exclusion Chromatography for Investigating Single Chain Folding − Current Status and Future Perspectives. *Polym. Chem.* **2019**, *10*, 3410−3425.
(51) Stefanidis, D.; Jencks, W. P. General Base Catalysis of Ester Hydrolysis. *J. Am. Chem. Soc.* **1993**, *115*, 6045−6050.
(52) Paramonov, S. E.; Bachelder, E. M.; Beaudette, T. T.; Standley, S. M.; Lee, C. C.; Dashe, J.; Fréchet, J. M. J. Fully Acid-Degradable Biocompatible Polyacetal Microparticles for Drug Delivery. *Bioconjugate Chem.* **2008**, *19*, 911−919.
(53) Amato, D. N.; Amato, D. V.; Mavrodi, O. V.; Martin, W. B.; Swilley, S. N.; Parsons, K. H.; Mavrodi, D. V.; Patton, D. L. Pro-Antimicrobial Networks Via Degradable Acetals (Pandas) Using Thiol−Ene Photopolymerization. *ACS Macro Lett.* **2017**, *6*, 171−175.
(54) Lutz, J.-F. Coding Macromolecules: Inputting Information in Polymers Using Monomer-Based Alphabets. *Macromolecules* **2015**, *48*, 4759−4767.
(55) Mai, Y.; Eisenberg, A. Self-Assembly of Block Copolymers. *Chem. Soc. Rev.* **2012**, *41*, 5969−5985.
(56) Alemán, J. V.; Chadwick, A. V.; He, J.; Hess, M.; Horie, K.; Jones, R. G.; Kratochvíl, P.; Meisel, I.; Mita, I.; Moad, G.; Penczek, S.; Stepto, R. F. T. Definitions of Terms Relating to the Structure and Processing of Sols, Gels, Networks, and Inorganic-Organic Hybrid Materials (Iupac Recommendations 2007). *Pure Appl. Chem.* **2007**, *79*, 1801.
(57) Pelipenko, J.; Kristl, J.; Rošic, R.; Baumgartner, S.; Kocbek, P. Interfacial Rheology: An Overview of Measuring Techniques and Its Role in Dispersions and Electrospinning. *Acta Pharm.* **2012**, *62*, 123−140.
(58) Langevin, D.; Monroy, F. Interfacial Rheology of Polyelectrolytes and Polymer Monolayers at the Air−Water Interface. *Curr. Opin. Colloid Interface Sci.* **2010**, *15*, 283−293.
(59) Li, J.; Wang, Y.; Wang, X.; Wu, D. Development of Polyoxymethylene/Polylactide Blends for a Potentially Biodegradable Material: Crystallization Kinetics, Lifespan Prediction, and Enzymatic Degradation Behavior. *Polymers* **2019**, *11*, 1516.
(60) Oyanagi, Y. Flow Behavior of High Polymers and Its Application to Polymer Processing. *J. Rheol.* **1994**, *38*, 761−762.
(61) Love, J. A.; Morgan, J. P.; Trnka, T. M.; Grubbs, R. H. A Practical and Highly Active Ruthenium-Based Catalyst That Effects the Cross Metathesis of Acrylonitrile. *Angew. Chem., Int. Ed.* **2002**, *41*, 4035−4037.
(62) Wang, X.; Hadjichristidis, N. Organocatalytic Ring-Opening Polymerization of N-Acylated-1, 4-Oxazepan-7-Ones toward Well-Defined Poly (Ester Amide) S: Biodegradable Alternatives to Poly (2-Oxazoline) S. *ACS Macro Lett.* **2020**, *9*, 464−470.

https://dx.doi.org/10.1021/acs.macromol.0c01051
Macromolecules XXXX, XXX, XXX−XXX